Microwave Synthesis of Noncentrosymmetric $BaTiO_3$ Truncated Nanocubes for Charge Storage Applications

V. Swaminathan,*,† Stevin S. Pramana,† T. J. White,†,‡ L. Chen,† Rami Chukka,† and R. V. Ramanujan*,†

School of Materials Science and Engineering, Nanyang Technological University, Singapore, 639798, and Centre for Advanced Microscopy, Australian National University, Canberra, ACT 2601

ABSTRACT Truncated nanocubes of barium titanate (BT) were synthesized using a rapid, facile microwave-assisted hydrothermal route. Stoichiometric composition of pellets of nanocube BT powders was prepared by two-stage microwave process. Characterization by powder XRD, Rietveld refinement, SEM, TEM, and dielectric and polarization measurements was performed. X-ray diffraction revealed a polymorphic transformation from cubic $Pm\bar{3}m$ to tetragonal $P4mm$ after 15 min of microwave irradiation, arising from titanium displacement along the *c*-axis. Secondary electron images were examined for nanocube BT synthesis and annealed at different timings. Transmission electron microscopy showed a narrow particle size distribution with an average size of 70 ± 9 nm. The remanence and saturation polarization were 15.5 ± 1.6 and 19.3 ± 1.2 $\mu C/cm^2$, respectively. A charge storage density of 925 ± 47 nF/cm^2 was obtained; Pt/BT/Pt multilayer ceramic capacitor stack had an average leakage current density of 5.78 ± 0.46 × 10^{-8} A/cm^2 at ±2 V. The significance of this study shows an inexpensive and facile processing platform for synthesis of high-*k* dielectric for charge storage applications.

KEYWORDS: $BaTiO_3$ • charge storage • memory devices • microwave hydrothermal synthesis • multilayer ceramic capacitor

1. INTRODUCTION

The ferroelectric $BaTiO_3$ (BT) is a widely studied high-*k* electroceramic that can be deployed in tunable microwave devices, thermistors, phase shifters, and multilayer ceramic capacitors (MCC) (1−5). Also, high-*k* BT is relevant in charge storage memory device applications such as dynamic random access memory (DRAM) that requires polarizability, piezoelectricity, pyroelectricity, and electro-optic activity (3, 6−8). However, the grain size control largely hinders the production of high capacitance devices, which is of great interest in dielectric oxide devices. In MCC, integration of BT on the upper and lower surfaces of certain metal substrates could replace existing dielectric materials such as SiO_2, e.g., in the Pt/SiO_2/Pt stack (9). Ferroelectric properties of BT can be tuned by changing the grain size (small crystals enhance performance of a device), resulting in high dielectric constant at room temperature (10).

Novel synthesis techniques are needed to control the shape and size of the BT nanomaterials to improve the ferroelectrics properties for high charge density capacitor applications. Key property metrics include charge storage capacity (11), electric field-dependent dielectric constant (12), leakage current density (13), and high-frequency losses. Typically, these properties are controlling the microstructure (14), grain size (15), and particle size distribution by appropriate sintering parameters and annealing conditions (16). BT undergoes a reversible crystallographic transformation upon heating above the Curie temperature ($T_c \approx 120$ °C) from the tetragonal $P4mm$ ($a = 3.9972 \pm 0.0005$) Å, $c = 4.041 \pm 0.001$) Å) (17, 18) to the cubic $Pm\bar{3}m$ ($a = 3.999$ Å) (19), because of the displacement of Ti^{4+} ions to the center of the TiO_6 octahedron. This transformation results in a change in dielectric constant values and thereby modifies the ferroelectric properties (20), which could also be tuned by adjusting the grain size (15).

Ferroelectric materials are usually synthesized by physical as well as chemical routes (21−27). Conventional methods, including radio frequency (RF) sputtering (21), pulsed laser deposition (PLD) (24), and metal organic chemical vapor deposition (MOCVD) are relatively expensive and low throughput (27), and have high maintenance costs, whereas high-temperature solid-state reactions produce submicrometer size crystals (28) and multiple calcinations, often require grinding steps, and are not suitable to obtain narrow particle size distributions. And, interestingly, these problems can be mitigated by low-cost chemical synthesis, in which preparation of tetragonal $P4mm$ BT nanoparticles of uniform composition with a wide range of cation substitutions is possible and the crystallinity is more easily controlled by chemical methods (17, 29, 30). BT has been synthesized at lower temperatures using or by metal salts or organometallic precursors by sol−gel (7), hydrothermal (29, 30), solvothermal (31), combustion (32), coprecipitation (33), and microwave hydrothermal methods (34, 35). Few researchers have

* Corresponding author. E-mail: ramanujan@ntu.edu.sg (R.V.R.); sviswanathan@ntu.edu.sg (V.S.).
Received for review June 4, 2010 and accepted September 15, 2010
† Nanyang Technological University.
‡ Australian National University.
DOI: 10.1021/am1004865

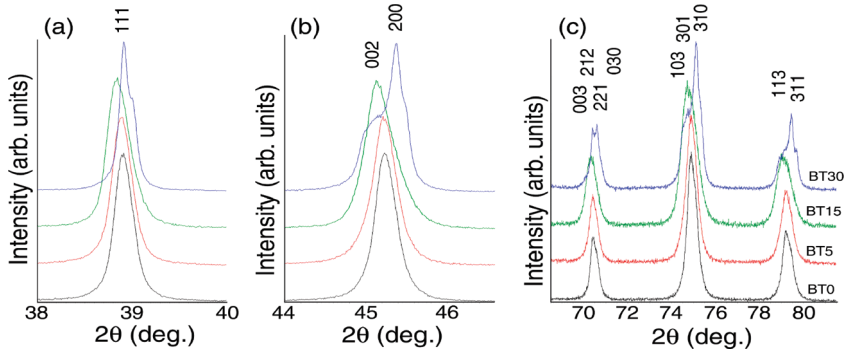

FIGURE 1. Closer inspection of XRD patterns of (a) {111}; (b) {200}; and (c) {300} and {221} (the $d_{300} = d_{211}$ in cubic), {031}, {311} Bragg's angles showing crystal structure transformation from cubic to tetragonal as the microwave heating time increases.

Table 1. Refined Crystal Parameters for Different Synthesized BT Crystals

	BT0	BT5	BT15	BT30
R_{wp}/R_b[a]	5.8/1.7	6.2/1.9	7.9/1.7	7.3/2.2
space group	$Pm\bar{3}m$	$Pm\bar{3}m$	$P4mm$	$P4/mmm$
a (Å)	4.00856	4.01043	4.00955	3.99834
	±0.00003	±0.00003	±0.00007	±0.00004
c (Å)			4.0274	4.02560
			±0.0001	±0.00005
volume (Å^3)	64.412	64.502	64.745	64.356
	±0.001	±0.002	±0.003	±0.001
c/a	1	1	1.0045	1.0068

[a] $R_{wp} = [(\sum_i w_i |y_{io} - y_{ci}|^2)/\sum_i w_i y_{io}^2]^{1/2}$ and $R_b = \sum_i I_{ko} - I_{kc}|/\sum_i I_{ko}$.

studied the effect of microwave frequency on hydrothermal synthesis of nanocrystalline tetragonal $BaTiO_3$; however, the structure and its ferroelectric properties were not clearly identified (31, 34, 35).

Microwave synthesis provides a combination of simplicity, energy efficiency, and high production rates and can produces nanoparticles with a narrow size distribution while avoiding high-temperature calcinations of 1000−1200 °C for several hours (31, 34, 35). In earlier reports, microwave hydrothermal and solvothermal techniques were used for the synthesis of semiconducting and oxide nanomaterials which exhibited excellent electronic (36) and optoelectronic properties (37, 38). Here the facile syntheses of tetragonal BT nanocube powders by microwave synthesis and annealing as well as their ferroelectric and dielectric properties are described.

2. EXPERIMENTAL SECTION

Materials. A domestic microwave oven operated at 2.45 GHz and with output power of up to 800 W and high-purity reagents barium nitrate (Sigma Aldrich, purity >99.99%), titanium isoproxide (Sigma Aldrich, purity ≥97%), nitric acid (ACS reagent 70%), ammonium hydroxide (Sigma Aldrich), and glycine (Sigma-Aldrich, purity >99%) were used for $BaTiO_3$ synthesis. Titanyl nitrate was prepared by dissolving titanium isopropoxide in ammonium hydroxide in an ice bath to form titanic acid to which nitric acid was then added.

Synthesis. The steps involved in the synthesis of $BaTiO_3$ are shown in Figure S1 in the Supporting Information. Using propellant chemistry concepts, we used glycine and nitrate as fuel and oxidizer, respectively. Although many reducing agents have been reported (39), glycine delivers the highest thermal energy and least carbon residue. Barium nitrate (0.05M) and titanyl nitrate (0.03M) were mixed and sonicated for 5 min, after which glycine was slowly added to form a viscous sol. The viscous sol pH was maintained at ∼2.1 by adding dil.HNO_3 or NH_4OH. The viscous sol was placed in a glass vessel, which is transparent to microwave irradiation (microwave transmitter), and irradiated for 2 min at 400 W in a microwave system (with a rotator) to produce homogeneous mixture of viscous sol; the irradiation was continued for 8 min at 400 W to initiate dehydration and evaporation of volatiles. Before auto combustion (ignition), the viscous sol temperature was 150−170 °C. After ignition, the flame temperature reached up to 1300 °C (40). Further irradiation (800 W/5 min) first converted the viscous sol to white foam, after which exothermic combustion initiated crystallization to finally yield a fine white oxide powder. The as-prepared powders were filtered and thoroughly washed with double-distilled water; dried powders were used for further analysis.

BT Pellet. BT powders were compacted at a pressure of 10 tons to produce 13 mm diameter and 2 mm thick pellets; then microwave irradiated at 800 W for 5 (BT5), 15 (BT15), and 30 (BT30) mins.

Characterization. Laboratory powder X-ray diffraction (XRD) patterns of BT were acquired at room temperature with a Bruker D8 diffractometer using Cu$K\alpha_1$ radiation over 10−130° 2θ, at a step size of 0.02° and dwell time of 0.6 s per step. The crystal structures of the BT polymorphs were refined by Rietveld analysis (41) as implemented in TOPAS version 3 (42) with a fundamental parameter peak shape profile (43) and the starting models for $Pm\bar{3}m$ (19), $P4mm$ (18), and $P4/mmm$ (44) employed. A three-coefficient Chebychev polynomial and $1/x$ background, a zero error, unit-cell parameters, scale factors, and crystal size/strain were refined sequentially. Isotropic temperature displacement factors were refined. Secondary electron images of BT nanocubes were examined by FESEM at 5 keV (JEOL-6340F). Powders for selected area electron diffraction (SAD) and high-resolution transmission electron microscopy (HRTEM) were prepared by grinding under ethanol, and drops of the suspension were deposited on holey carbon-coated copper grids. Images were collected with a JEOL-2100F microscope operated at 200 kV using a low-background Gatan double tilt holder.

Electric, dielectric, and ferroelectric properties were monitored as a function of composition. An MCC stack was fabricated by sputter coating a platinum layer (500 nm) on the upper and lower surfaces of the BT pellet. The ferroelectric properties and leakage current were measured (11) using a Signatone probe station and Teck 609 × 10^{-6} high voltage amplifier coupled with a Radiant EF Technology precision LC materials analyzer. Current−voltage measurements were performed using a 610-Keithley electrometer and a variable Aplab DC voltage source.

Table 2. Refined Atomic Parameters and Selected Ti−O Bond Lengths (Å) in the Distorted TiO_6 Octahedron for *P4mm* BT15

atom	Wyckoff position	fractional coordinate *z*	B_{eq} (Å^2)
Ba_1	1a (0, 0, *z*)	−0.0001 ± 0.0006	0.31 ± 0.01
Ti_1	1b (1/2, 1/2, *z*)	0.5267 ± 0.0006	0.24 ± 0.02
O_1	1b (1/2, 1/2, 1/2)*	0	0.30 ± 0.02
O_2	2c (1/2, 0, *z*)*	0.5	0.30 ± 0.01

bond between atoms	bond length (Å)
Ti−O_1	1.91
Ti−O_1	2.12
Ti−O_2 (×4)	2.01

* Fractional coordinate 'z' for O_1 and O_2 was not refined.

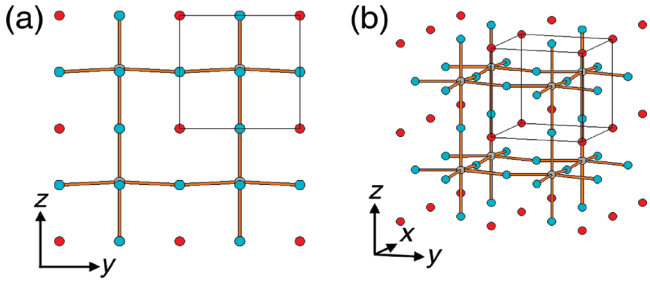

FIGURE 2. Structural drawing of BT15 crystallized in *P4mm* (a) oriented along [100] and (b) clinographically oriented along [100]. Ti (gray) is displaced 0.11 Å along *z* to create polarization while Ba and O are shown in red and blue, respectively. Unit cell is outlined with a box.

3. RESULTS AND DISCUSSION

The synthesis process of microwave and conventional hydrothermal synthesis are fundamentally different. In microwave synthesis, the reactants (susceptor) absorb microwaves and thereby generate heat within them. Because of this generated heat, the reaction can occur in a few minutes that greatly increase reaction kinetics, leading to rapid formation of BT nanocube powders.

The heating resulted in exothermic reaction, which facilitated the nucleation and growth of BT powders (eq 1).

$$2Ba(NO_3)_{3(aq)} + 2TiO(NO_3)_{2(aq)} + 8C_2H_5NO_{2(aq)} + 5O_{2(g)} \rightarrow 2BaTiO_{3(s)} + 9N_{2(g)} + 16CO_{2(g)} + 20H_2O_{(g)} \quad (1)$$

The as-synthesized BT powders and pellets were characterized by XRD. A closer inspection of XRD pattern of powder and pellet BT show that the extent of the cubic to tetragonal polymorphic transformation increased with irradiation time (Figure 1). For BT0 and BT5, respectively, the reflections at $2\theta = 38.8$ and 45° are single symmetric peaks consistent with $Pm\bar{3}m$ (Figure 1 and Table S1 in the), the small crystallite size of 43 ± 9 nm may stabilize the cubic structure at room temperature (33, 45), even though the tetragonal polymorph is usually reported. BT pellets irradiated for intermediate times (BT15) were initially refined in $Pm\bar{3}m$ to yield residuals R_{wp} and R_b of 8.9 and 2.0%, respectively. Although slight {*h*00} peak asymmetry suggests the material is not isometric, Rietveld analysis using centrosymmetric *P4/mmm* and noncentrosymmetric *P4mm* models yielded insignificant differences. CCDC 774808−774811 contains the supplementary crystallographic data for this paper. These data can be obtained free of charge from The Cambridge Crystallographic Data Centre (CCDC) via www.ccdc.cam.ac.uk/data_request/cif.

The possibility of a tetragonal/cubic mixture cannot be discounted, but the resolution of the XRD pattern cannot

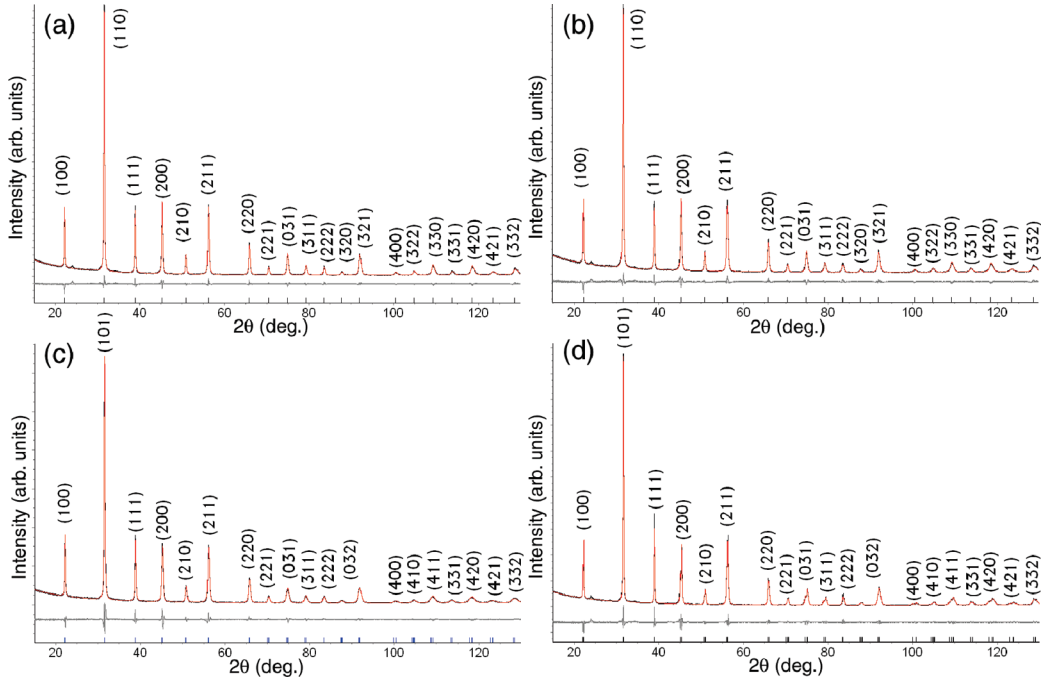

FIGURE 3. Rietveld plot of the XRD data of (a) BT0, (b) BT5, (c) BT15, and (d) BT30 collected at room temperature. The observed intensity is shown in black, with the red line representing the calculated intensity. Differences between observed and calculated intensities are plotted beneath. Vertical markers indicate the Bragg reflections.

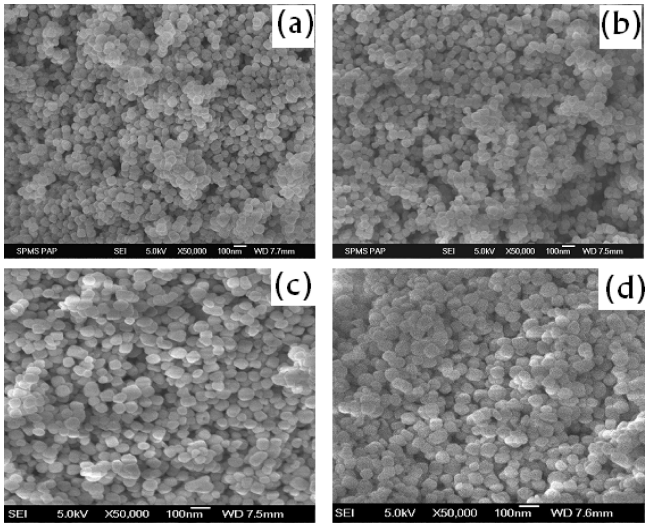

FIGURE 4. Secondary electron images examined at 5 keV at 50 000× magnification for different microwave irradiation: (a) BT 0 (average particles size of 40 ± 6 nm), (b) BT 5 (average particles size of 50 ± 5 nm), (c) BT 15 (average particles size of 70 ± 7 nm), (d) BT 30 (average particles size of 85 ± 7 nm).

remove ambiguity on this point. Large polarization in BT15 (described in the following section) is consistent with the absence of a center of symmetry.

A *c*/*a* ratio of 1.0045 for BT15 when refined in *P*4*mm* was calculated (R_{wp} = 7.9% and R_b = 1.7%) with a Ti displacement along [001] of 0.11 Å (Tables 1 and 2, Figure 2). The oxygen displacement along the *c*-axis could not be successfully modeled as negative atomic displacement parameters (ADPs) resulted. It is presumed the contribution from heavy Ba to the XRD pattern masks the position of low atomic number oxygen. Peak splitting of $\{h00\}/\{00l\}$ became more apparent for BT30 as expected for a tetragonal metric. Using the *P*4*mm* model for BT15 as a starting point led to negative ADPs for Ti, which was resolved by adopting centrosymmetric *P*4/*mmm* (Figure 3 and Table S2 in the Supporting Information).

Figure 4 shows the secondary electron images of nanocube BT synthesis and annealed at different timings in microwave irradiation. Grain growth vs microwave annealing studies of nanocube BT was examined at 800 W for 5−30 min. Figure 4a shows the as-synthesized nanocube BT0 of average particle size of 40 ± 6 nm was measured. The average grain size increased with microwave annealing time from 5 to 30 min; nanocube densification and minimized grain growth with average particles size of 50 ± 5 nm to 70 ± 7 nm was observed (Figure 4b,c). This results show that the short time is an essential factor to obtain BT nanocube with nanometer grain growth in this process; also we found exaggerated grain growth to 2-fold increment for BT 30 annealed pellets (Figure 4d). The density of as-prepared pellet was 5.32 g/cm^3 (87% of theoretical density); after microwave annealing, the pellet density increases to 5.38 for 5 min (88% of theoretical density) and 5.51 g/cm^3 for 15 and 30 min (91% of theoretical value). Particle size is bigger when the microwave irradiation time increases (Figure 4a−d).

Figures 5a−c illustrates the morphology and narrow size distribution of the $BaTiO_3$ crystals where cross-lattice graph, dislocations, and twinning were not observed. Further, particle agglomeration was not noticed, and the average crystal size was 70 ± 9 nm, consistent with XRD results. The SAD can be indexed with *P*4/*mmm* with $a = b = 4.01$ Å and $c = 4.03$ Å (Figure 5d).

High-*k* dielectric measurements were collected at room temperature from 100 Hz to 1 × 10^5 Hz for BT pellets. A maximum dielectric constant of 1068 (BT15) and less than 250 (BT0, BT5 and BT 30), independent of frequency (46), was observed. As the grain size and symmetry of BT 15 is optimal, the dielectric constant reaches 7903 at 120 °C for 100 Hz. This performance is superior to the earlier report as tabulated in Table 3 (47−49).

Although theBT15 sample had a maximum capacitance density of 925 ± 47 nF/cm^2, the other samples BT5 and BT30 exhibited a low capacitance density (Figure 6). A very

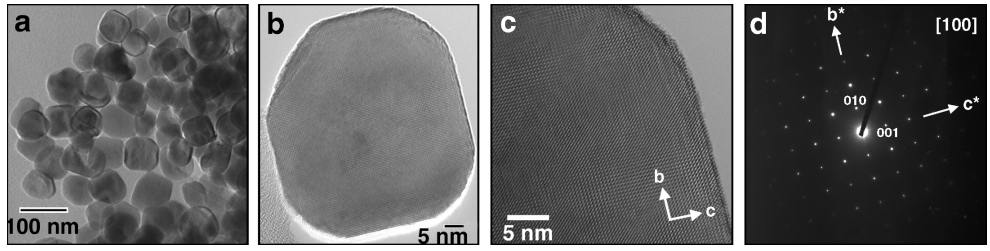

FIGURE 5. (a) BT15 truncated nanocube distribution; (b) bright-field image; and (c) HRTEM of a single crystal aligned along [100]; (d) corresponding SAED of c.

Table 3. Properties of BT Powders Prepared by Different Methods

methods of materials processing	Caballero et al. (47)	Yuan et al. (48)	Cernea (49)	this work
method	BT commercial grade	solid state method	sol gel	microwave hydrothermal
calcination/sintering	1250 °C(30 min)/1350 °C	800 and 1150 °C/1120 °C (2 h)	950 °C in air/1275 °C	no calcination/microwave annealing (5−30 min)
dielectric constant (maximum)	7500(1kHz)	8100 (1 kHz) with NBT doping	3020	7930 (100 Hz)- no doping
crystallite size (nm)			80	70 ± 9

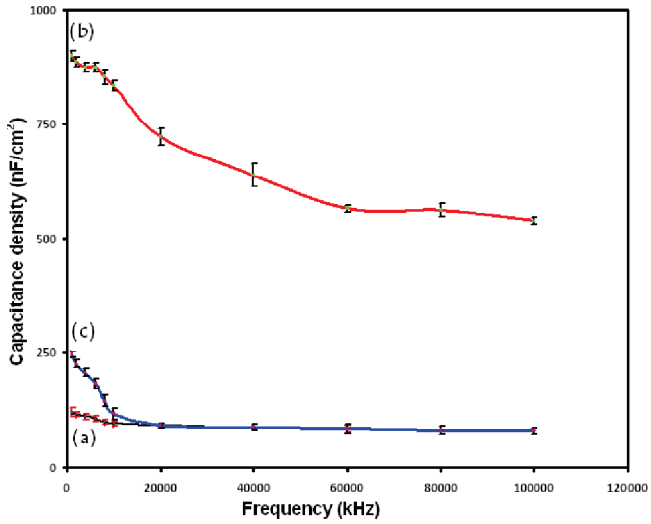

FIGURE 6. MCC stack of sputtered coating a platinum layer (500 nm) on the upper and lower surfaces of the BT pellet. Capacitance measurements of microwave synthesized/annealed nanocube BT for different microwave irradiation: (a) BT5, (b) BT15, and (c) BT30.

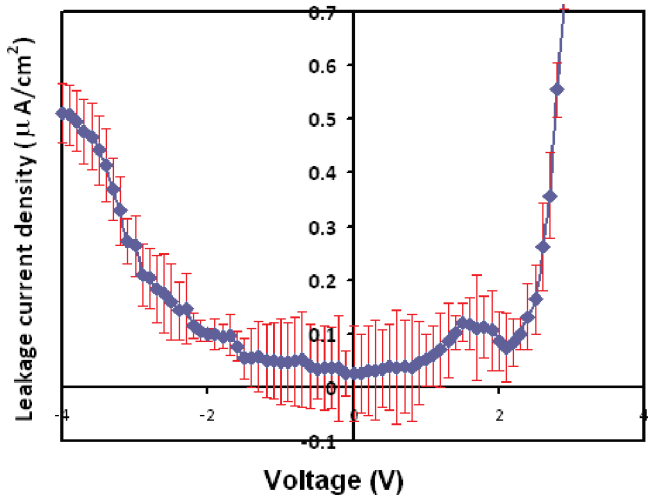

FIGURE 7. Voltage vs leakage current characteristics of nanocube BT pellet annealed at microwave power of 800 W for 15 min (BT 15).

high capacitance value obtained for BT15 is mainly due to the reduced crystal size (50). We assume that the lower capacitance value for other samples could be due to the polarization. Figure 7 shows the average leakage current density for sample BT15 is $5.78 \pm 0.46 \times 10^{-8}$ at ± 2 V (1×10^{-8} A/cm^2 at 0 V) (51), which is lower than previously observed values (11, 13). Liao et al. have produced a metal−insulator−metal (MIM) capacitor with leakage current of less than 4×10^{-5} A/cm^2 (11).

The hysteresis loop for a Pt/BT/Pt capacitor stack annealed at 800 W for different durations is shown in Figure 8. A maximum remanence of 15.5 ± 1.6 μC/cm^2 and saturation polarization of 19.3 ± 1.2 μC/cm^2 was obtained for BT15. We note here that these values are reasonably comparable to the maximum switching charge density of FeRAM devices (52). Therefore, BT nanocubes synthesized by microwave annealing process for a short period of preparation time, optimized size and structure, and desired composition are suitable for making MIM/metal-capacitor-

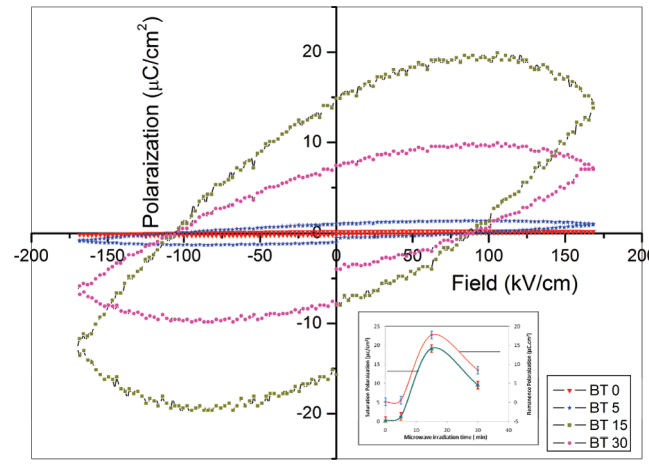

FIGURE 8. Hysteresis loop of nanocube BT pellets annealed at 800 W of microwave irradiation for different durations: (a) BT0, (b) BT5, (c) BT 15, and (d) BT 15.

metal (MCM) stacks; such devices display Curie−Weiss behavior comparable to Wang et al. (53) where crystal sizes below 44 nm did not exhibit ferroelectricity. Produced BT nanocube results of XRD and SEM were supported the polarization results of BT15 samples. Thus, the BT 15 pellet showed superior ferroelectric properties, whereas BT0 and BT5 did not because of the cubic crystal structure in nature and BT 30 had high strain centrosymmetry.

4. CONCLUSIONS

Tetragonal structured $BaTiO_3$ (BT) nanocube powders were successfully produced by a facile microwave synthesis technique. Microwave synthesis and rapid annealing of BT nanocube improves overall density and minimizes the grain growth with shorter processing time produced a cheaper MCC electrode. Microwave irradiation resulted in a dimorphic phase transformation from the cubic to the tetragonal structure. Grain growth vs microwave annealing studies was examined for nanocube BT. Minimize grain growth and densification with average particles size of 70 ± 7 nm for BT microwave annealed at 800 W for 15 min. Truncated BT nanocubes of cross section 70 ± 9 nm in [100] projection was observed by TEM. BT pellet irradiated at 800W for 15 min, revealed a dielectric constant of 1068 at room temperature, while it was as high as 7903 (after annealing) at 120 °C. The Pt/BT/Pt MCC stack showed an average leakage current density of $5.78 \pm 0.46 \times 10^{-8}$ A/cm^2 at ±2 V. The hysteresis loop for BT nanocube irradiated for 15 min showing a remanence and saturation polarization of 15.5 ± 1.6 and 19.3 ± 1.2 μC/cm^2, respectively. From the experimental results, the $BaTiO_3$ nanocubes prepared in this study showed superior ferroelectric properties, which make them suitable for incorporation in charge storage devices.

Supporting Information Available: Experimental procedures; refined atomic parameters for barium titanate (BT) microwave annealed for 0, 5, and 30 min (PDF). This material is available free of charge via the Internet at http://pubs.acs.org.

REFERENCES AND NOTES

(1) Fang, C. Y.; Randal, C. A.; Lanagan, M. T.; Agrawal, D. K. *J. Electroceram.* **2009**, *22*, 125.
(2) Polotai, A. V.; Jeong, T. H.; Yang, G. Y.; Dickey, E. C.; Randall, C. A.; Pinceloup, P.; Gurav, A. S. *J. Electroceram.* **2009**, *23*, 6.
(3) Hsu, K. C.; Ying, K. L.; Chen, L. P.; Yu, B. Y.; Wie, W. C. J. *J. Am. Ceram. Soc.* **2005**, *88*, 524.
(4) Tsurumi, T.; Hoshina, T.; Takeda, H.; Mizuno, Y.; Chazono, H. *IEEE Trans. Ultrason., Ferroelectr., Frequency Control* **2009**, *56*, 1513.
(5) Yang, G.; Yuer, Z.; Sun, T.; Zhao, J.; Yang, Z.; Li, L. *Appl. Phys. A: Mater. Sci. Process.* **2008**, *91*, 119.
(6) Kulwicki, B. M. *J. Phys. Chem. Solids* **1984**, *45*, 1015.
(7) Blanco-Lopez, M. C.; Rand, B.; Riley, F. L. *J. Eur. Ceram. Soc* **1997**, *17*, 281.
(8) Gomez-Yanez, C.; Ramirez, B. H.; Martinez, F. *Ceram. Int.* **2000**, *26*, 609.
(9) Wang, J.; Zhang, T.; Xiang, J.; Li, W.; Duo, S.; Li, M. *J. Mater. Sci: Mater. Electron.* **2009**, *20*, 44.
(10) Frey, M. H.; Payne, D. A. *Appl. Phys. Lett.* **1993**, *63*, 2753.
(11) Liao, E. B.; Choong, T. H.; Zhu, W. G.; Teoh, K. W.; Lim, P. C.; Lo, G. Q.; Kwong, D. L. *IEEE Electron. Dev. Lett.* **2008**, *29*, 31.
(12) Ahmad, T.; Kavitha, G.; Narayana, C.; Ganguli, A. K. *J. Mater. Res.* **2005**, *20*, 1415.
(13) Kamel, F. E.; Gonon, P.; Radnoczi, G. *J. Appl. Phys.* **2009**, *105*, 074104.
(14) Ohno, T.; Suzuki, D.; Suzuki, H.; Ida, T. *Kona* **2004**, *22*, 195.
(15) Hsiang, H. I.; Yen, F. S. *J. Am. Ceram. Soc.* **1996**, *79*, 1053.
(16) Liou, Y. C.; Wu, C. T.; Chung, T. C. *J. Mater. Sci.* **2007**, *42*, 3580.
(17) Mandal, T. K. *Mater. Lett.* **2007**, *61*, 850.
(18) Smith, M. B.; Page, K.; Siegrist, T.; Redmond, P. L.; Walter, E. C.; Seshadri, R.; Brus, L. E.; Steigerwald, M. L. *J. Am. Chem. Soc.* **2008**, *130*, 6955.
(19) Miyake, S.; Ueda, R. *J. Phys. Soc. Jpn.* **1947**, *2*, 93.
(20) Leonard, M. R.; Safari, A. *IEEE Int. Symp. Appl. Ferroelectr.* **1996**, *2*, 1003.
(21) Kim, J. H.; Hishita, S. *J. Mater. Sci.* **1995**, *30*, 4645.
(22) Song, S. J. Z.; Yao, X. *Mater. Sci Eng., B* **2007**, *145*, 28.
(23) Sun, W.; Li, J. *Mater. Lett.* **2006**, *60*, 1599.
(24) Norton, M. G.; Carter, C. B. *J. Mater. Res.* **1990**, *5*, 2762.
(25) ParkerE. H. C. *The Technology and Physics of Molecular Beam Epitaxy*; Plenum: New York, 1986.
(26) Nagai, M.; Yamashita, K.; Umegaki, T.; Takuma, Y. *J. Am. Ceram. Soc.* **1993**, *76*, 253.
(27) Benomar, W. O.; Xue, S. S.; Lessard, R. A.; Singh, A. *J. Mater. Res.* **1994**, *9*, 970.
(28) Kumara, P.; Singh, S.; Spah, M.; Juneja, J. K.; Prakashe, C.; Raina, K. K. *J. Alloys and Comp* **2010**, 489.
(29) Asiaie, R.; Zhu, W.; Akbar, S. A.; Dutta, P. K. *Chem. Mater.* **1996**, *8*, 226.
(30) Newalkar, B. L.; Komarneni, S.; Katsuki, H. *Mater. Res. Bull.* **2001**, *36*, 2347.
(31) Chen, D.; Jiao, X. *J. Am. Ceram. Soc.* **2000**, *83*, 2637.
(32) Alexander, G. M. *J.Mater.Chem* **2004**, *14*, 1779.
(33) Li, X.; Shih, W. H. *J. Am. Ceram. Soc.* **1997**, *80*, 2844.
(34) Ying, M.; Elizabeth, V.; Steven, L. S.; Dutta, P. K. *Chem. Mater.* **1997**, *9*, 3023.
(35) Edward, K. N.; Chun-Hu, C.; Dutta, P. K.; Steven, L. S. *J. Phys. Chem. C* **2008**, *112*, 9659.
(36) Swaminathan, V.; Heng, O. Y.; Murugan, A. V. *J. Mater. Sci.* **2006**, *41*, 1459.
(37) Murugan, A. V.; Viswanath, A. K.; Kakade, B. A.; Swaminathan, V.; Ravi, V. *Appl. Phys. Lett.* **2006**, *89*, 123120.
(38) Murugan, A. V.; Viswanath, A. K.; Kakade, B. A.; Ravi, V.; Swaminathan, V. *J. Phys. D., Appl. Phy.s* **2006**, *39*, 3974.
(39) Bhame, S. D.; Swaminathan, V.; Deheri, P. K.; Ramanujan, R. V. *Adv. Sci. Lett.* **2010**, *3*, 174.
(40) Chick, L. A.; Pederson, L. R.; Maupin, G. D.; Bates, J. L.; Thomas, L. E.; Exarhos, G. J. *Mater. Lett.* **1990**, *10*, 6.
(41) Rietveld, H. *J. Appl. Crystallogr.* **1969**, *2*, 65.
(42) *TOPAS, version 3*; Bruker AXS Inc.: Madison, WI, 2005.
(43) Cheary, R. W.; Coelho, A. *J. Appl. Crystallogr.* **1992**, *25*, 109.
(44) Megaw, H. D. *Proc. R. Soc. London* **1947**, *189*, 261.
(45) Uchino, K.; Sadanaga, E.; Hirose, T. *J. Am. Ceram. Soc.* **1989**, *72*, 1555.
(46) Sharma, B. H.; Mansingh, A. *J. Phys. D: Appl. Phys.* **1998**, *31*, 1527.
(47) Caballero, A. C.; Feernandez, J. F.; Moure, C.; Duran, P.; G.Fierro, J. L. *J. Eur. Ceram. Soc.* **1997**, *17*, 513.
(48) Yuan, Y.; Zhang, S. R.; Zhou, X. H.; Tang, B. *J. Electron. Mater.* **2009**, *38*, 706.
(49) Carnea, M. *J. Optoelectron. Adv. Mater.* **2007**, *7*, 3015.
(50) Guo, N.; DiBenedetto, A. S.; Tewari, P.; Lanagan, T. M.; Ratner, M. A.; Marks, T. J. *Chem. Mater.* **2010**, *22*, 1567.
(51) Luborsky, F. E. *J. Appl. Phys.* **1961**, *32*, 171.
(52) *The International Technology Roadmap for Semiconductors*; Semiconductor Industry Association: San Jose, CA, 2003; Front End Processes Section, p 50.
(53) Wang, Y. G.; Zhong, W. L.; Zhang, P. L. *Solid State Commun.* **1994**, *90*, 329.

AM1004865